ACS NANO
Cite This: ACS Nano XXXX, XXX, XXX–XXX
www.acsnano.org

ARTICLE

Steering Coacervation by a Pair of Broad-Spectrum Regulators

Shenyu Yang,[†] Bo Li,[‡] Chunxian Wu,[§] Weiwei Xu,[†] Mei Tu,[*,†] Yun Yan,[∥] Jianbin Huang,[∥] Markus Drechsler,[⊥] Steve Granick,[‡,#] and Lingxiang Jiang[*,†,‡]

[†]College of Chemistry and Materials Science, Jinan University, Guangzhou 510632, China
[‡]Center for Soft and Living Matter, Institute for Basic Science (IBS), Ulsan 44919, Republic of Korea
[§]School of Chemistry and Chemical Engineering, Guangdong Pharmaceutical University, Zhongshan 528458, China
[∥]College of Chemistry and Molecular Engineering, Peking University, Beijing 100871, China
[⊥]Bavarian Polymer Institute (BPI), Laboratory for Soft-Matter Electron Microscopy, University of Bayreuth, D-95440 Bayreuth, Germany
[#]Departments of Chemistry and Physics, UNIST, Ulsan 44919, Republic of Korea

Supporting Information

ABSTRACT: **Coacervation is liquid–liquid phase separation ubiquitous in industrial applications and cellular biology. Inspired by cellular manipulation of coacervate droplets such as P granules, we report here a regulatory strategy to manipulate synthetic coacervation in a spatiotemporally controllable manner. Two oppositely charged small molecules are shown to phase separate into coacervate droplets in water as a result of electrostatic attraction, hydrophobic effect, and entropy. We identify a down regulator, β-cyclodextrin, to disrupt the hydrophobic effect, thus dissolving the droplets, and an up regulator, amylase, to decompose β-cyclodextrin, thus restoring the droplets. The regulation kinetics is followed in real time on a single-droplet level, revealing diffusion-limited dissolution and reaction-limited condensation, respectively, taking ∼4 s and 2–3 min. Versatility of this strategy to manipulate the coacervation is demonstrated in two aspects: spatially distributed coacervation in virtue of amylase-grafted hydrogel frameworks and coacervate transportation across membranes and hydrogel networks *via* a disassemble-to-pass strategy. The current regulatory pairs and strategies are anticipated to be general for a wide variety of synthetic self-assembly systems.**

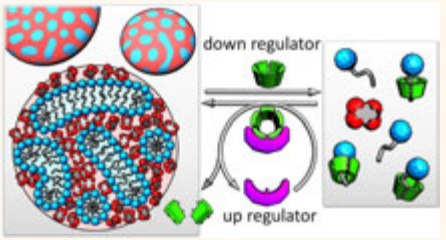

KEYWORDS: *coacervation, regulators, cyclodextrin, transportation, patterning, enzymes, biomimicry*

Cells have mastered a sophisticated self-assembly strategy to construct structures and organelles and, more importantly, to regulate them in a spatiotemporally precise manner in response to life cycles or external stimuli.[1] For example, a cell moves by deploying different regulatory proteins to polymerize and depolymerize actin filaments at the motion front and rear, respectively.[1] During a division cycle of *Caenorhabditis elegans* embryo cells, P granules (membraneless assemblies or coacervates of different RNA and proteins) start off with a uniform distribution across the cytoplasm, then dissolve evenly as regulated by MEX-5 that competes with RNA, and end up with condensation at the posterior half due to the localized PAR-1 that depletes nearby MEX-5 (Scheme 1a).[2] This spatiotemporal manipulation enables the cell to unsymmetrically divide into a somatic and a germ daughter, and such division repeats to preserve the germ line during embryo development. Such cellular manipulation with spatiotemporal precision and functional complexity is, however, yet to be paralleled in synthetic self-assembly systems.

Coacervation is a type of liquid–liquid phase separation driven by intermolecular interactions or entropy to produce coacervate droplets.[3−8] These droplets were extensively studied in basic science, such as permeable compartmentalization,[9−11] fiber incubation,[12−14] protocell modeling,[15−17] and cellular biology,[18−22] and were widely applied in industries including cosmetics, food, and pharmaceutics.[3] Of particular relevance here is their high reconfigurability in response to environmental or chemical changes as a result of their membraneless boundaries and liquid nature. It is, for example, encouraging to notice the (de)phosphorylation-mediated reversible coacervation recently reported by Keating *et al.*[23,24] In this paper, we identify a pair of broad-spectrum regulators for synthetic coacervation systems and develop strategies to manipulate them for patterning and transportation.

Received: December 10, 2018
Accepted: January 31, 2019
Published: January 31, 2019

DOI: 10.1021/acsnano.8b09332
ACS Nano XXXX, XXX, XXX–XXX

Scheme 1. Experimental Design[a]

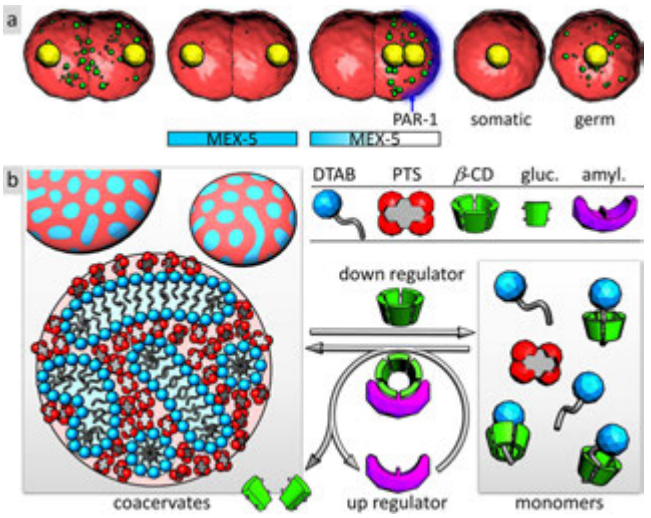

[a]Conditions: (a) During an unsymmetrical cellular division, P granules (green spheres) start with a uniform distribution across the cytoplasm, then dissolve evenly in the presence of MEX-5, and selectively condensate at the posterior half as a result of depletion of MEX-5 caused by localized PAR-1. Eventually, one daughter is somatic and free of the P granule, and the other one is germ and rich in P granule. (b) Oppositely charged DTAB and PTS form coacervate droplets at a near-neutral ratio as a result of hydrophobic effect, electrostatic attraction, and entropy. Inside a droplet, DTAB molecules arrange themselves into threadlike micelles to separate the hydrophobic region (blue) from the hydrophilic region (pink). As a down regulator, β-CD disassembles the droplets by extracting DTAB from the droplets into its cavity. As an up regulator, amylase reassembles the droplets by decomposing β-CD into glucose.

Our design involves two ingredients for coacervation and two regulators (Scheme 1b): dodecyltrimethylammonium bromide (DTAB; see Figure S1 for molecular structures), pyrenetetrasulfonate tetrasodium (PTS), β-cyclodextrin (β-CD), and amylase. β-CD can extract DTAB into its cavity, thus dissolving the droplets, and amylase can decompose β-CD to release DTAB, thus restoring the droplets. Although the MEX-5/PAR-1 pair is specific for the P granule, the β-CD/amylase pair is expected to be broadly effective for amphiphilic self-assemblies because the CD cavity can bind various hydrophobic groups. We then use this coacervation regulation to realize spatially controlled formation/dissolution of coacervates with a hydrogel framework and transportation of coacervates through porous membranes and hydrogels.

RESULTS AND DISCUSSION

Coacervation of DTAB and PTS. In a previous work, we studied the surface properties of DTAB/PTS mixtures in detail but only preliminarily explored their coacervation behavior.[25] We thus lay out a more systematic characterization here. DTAB has a hydrophobic tail and a positively charged headgroup, whereas PTS has a pyrene core and four negatively charged groups on the rim. Mixing DTAB and PTS at a near-neutral ratio produces massive droplets that turn the clear solution into a turbid, fluorescently cyan suspension, typical for liquid−liquid phase separation (Figure S2a). The fluorescence comes from the pyrene core of PTS that emits cyan and blue light in aggregated and monomeric forms, respectively (Figure S3). The droplets gradually coalesce and sediment into a bottom phase rich in DTAB and PTS (Figure S2b).

Before complete coalescence, we identify round droplets ranging from 2 to 10 μm (Figure 1a,b). Cryogenic transmission electron microscopy (cryo-TEM) images at an early stage of coacervation show ~100 nm droplets often in the process of coalescence (Figure 1c). Scrutiny of a single droplet (Figure 1d) reveals rich inner textures with approximately equal amounts of dark and light regions intertwining with each other, reminiscent of spinodal decomposition patterns.[26] The dark or light regions are composed of threads and branches with a thickness ~2.3 nm, twice the length of DTAB molecules. We thus speculate a further phase separation inside the droplets where DTAB molecules form threadlike micelles to segregate the hydrophobic tails from the hydrophilic regions full of charged groups and water (Scheme 1).

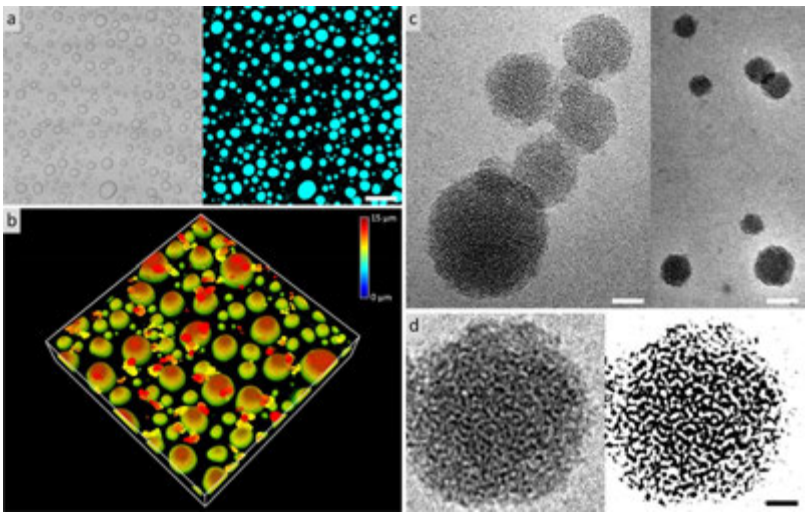

Figure 1. Microscopic pictures of the DTAB/PTS coacervate droplets. (a) Confocal images of the droplets in white light and fluorescence modes. Scale bar = 15 μm. (b) 3D confocal scan of the droplets on a glass surface. Scanning box = 70 × 70 × 15 μm. Color bar indicates height in z axis. (c) Cryo-TEM pictures of newly formed droplets that are coalescing. Scale bars = 40 (left) and 80 (right) nm. (d) Single droplet with its inner textures enhanced on the right. Scale bar = 20 nm.

DOI: 10.1021/acsnano.8b09332
ACS Nano XXXX, XXX, XXX−XXX

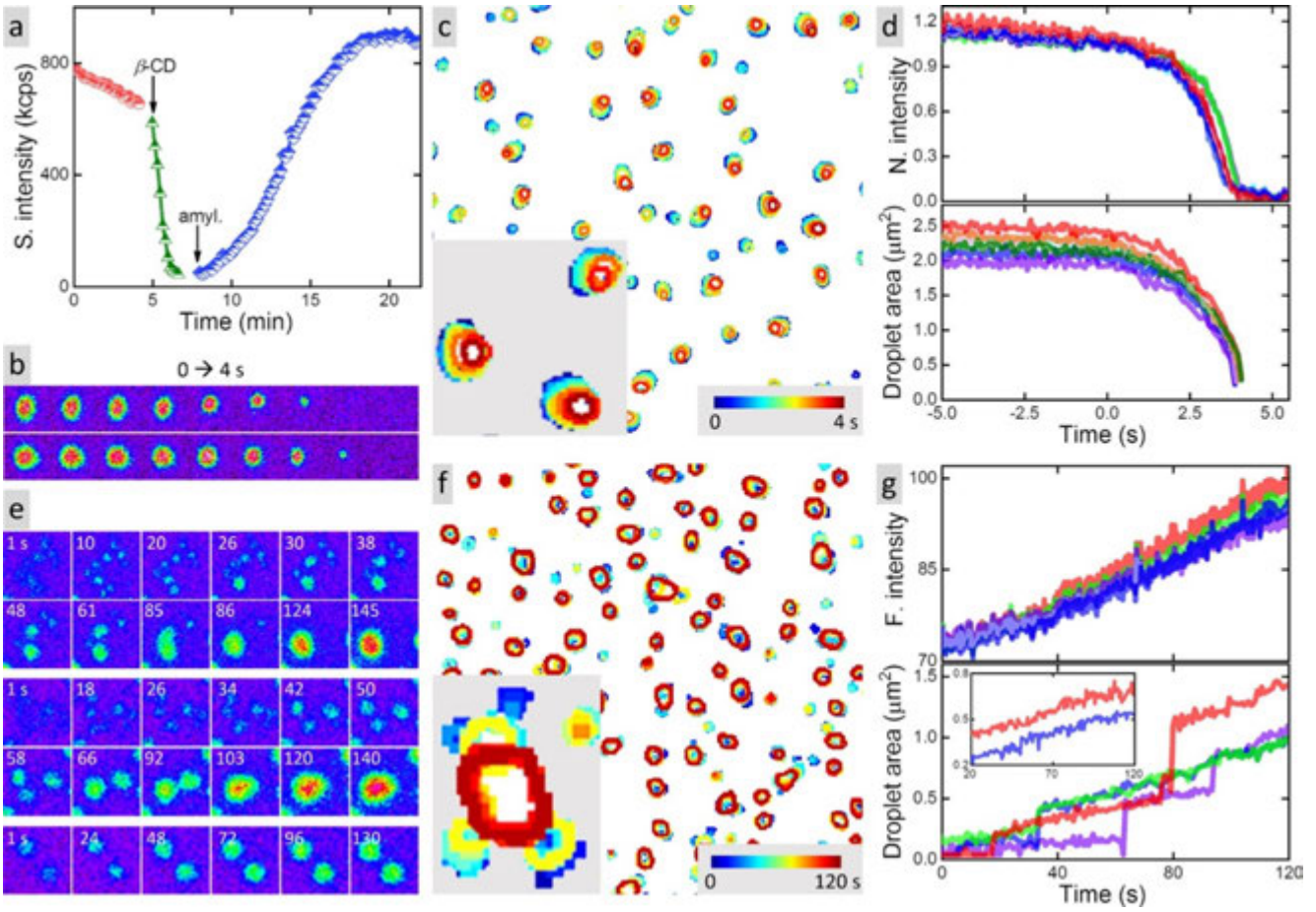

Figure 2. Coacervation regulation by β-CD and amylase. (a) Scattering intensity of a DTAB/PTS suspension as a function of time with the arrows indicating β-CD or amylase addition. The sample is held at 55 °C in this the entire experiment for enzymatic activity. (b–d) Dissolution kinetics followed on single-droplet level, showing two 3.2 × 3.2 μm regions of interest (ROIs) (b), a 25 × 25 μm map of color-coded droplet contours (c), and time dependence of normalized fluorescence intensity of ROIs and droplet area (d) as a function of time. (e–g) Condensation kinetics followed on single-droplet level. The ROIs in (e) are 4.5 × 4.5 μm, and the map in (f) is 25 × 25 μm. The droplet area jumps at merging events but increases linearly otherwise (g), where the inset shows droplet area curves for cases of simple expansion.

Regulation of Coacervation by β-CD and Amylase. As a donut-like oligosaccharide with a hydrophilic outer surface and a hydrophobic cavity, β-CD can thread the hydrocarbon chain of DTAB into its cavity in a 1:1 stoichiometry with a high binding constant of $\sim 2 \times 10^4$ M^{-1}.[27−29] Addition of β-CD to a DTAB/PTS mixture dissolves the coacervates and produces a clear, fluorescently blue solution (Figure S2c). Two other cyclodextrins, α-CD and γ-CD, have a similar effect on DTAB/PTS coacervation. Macroscopic dissolution of the droplets finishes within 2 min (Figure 2a). α-Amylase is an enzyme that cleaves α-1,4 linkages between glucose units of linear and cyclic starch molecules such as CDs.[30−32] Incubation of amylase in a DTAB/PTS/β-CD solution slowly degrades β-CD and releases DTAB to re-form the coacervate droplets in ~10 min (Figure 2a). The enzymatic reaction reaches optimum efficiency at 55 °C but barely proceeds at 25 °C (Figure S4a), providing us a convenient handle to activate or deactivate amylase. Amylase activity is moderate for β-CD and γ-CD but quite low for α-CD that is too small to fit in the enzymatic binding site (Figure S4b).[32]

We follow the dissolution and condensation on glass surfaces in real time on single-droplet level. In dissolution experiments, a concentrated β-CD solution is gently injected onto the top layer of a coacervate suspension. After a waiting period for β-CD to diffuse to the sample−glass surface, the droplets start to shrink dramatically (Movie S1). Droplet contours are tracked during the process (Figure 2c), where droplet shrinkage and centroid shifting are notable. Figure 2b highlights time sequences of two regions of interest (ROIs) of the original movie. Single-droplet tracking suggests that most of the droplets are synchronized to vanish within a short time of ~4 s (Figure 2d). In condensation experiments, the DTAB/PTS/β-CD/amylase mixture is heated to 55 °C to initiate the enzymatic reaction while a video is recorded (Movie S2). A time-coded map of droplet contours demonstrates droplet expansion and frequent merging events in 120 s (Figure 2f). Figure 2e highlights stepwise merging events (for example, 6 small droplets gradually turns into one big droplet in the two top rows), vanishing events (the two top-right droplets fully disappear at 124 s in the two top rows), and simple expansion without merging (the lower row). Interestingly, although fluorescence intensity of a ROI increases constantly and linearly irrespective of merging events, droplet area tracking picks up the merging events nicely (Figure 2f). For a single droplet, its dissolution and condensation are presumably limited by β-CD diffusion (~4 s) and by β-CD decomposition (2−3 min), respectively.

Spatiotemporal Regulation. In a naïve attempt to realize spatially controlled coacervation, we built an asymmetrical chamber with half of its bottom glass coated by amylase and the

DOI: 10.1021/acsnano.8b09332
ACS Nano XXXX, XXX, XXX−XXX

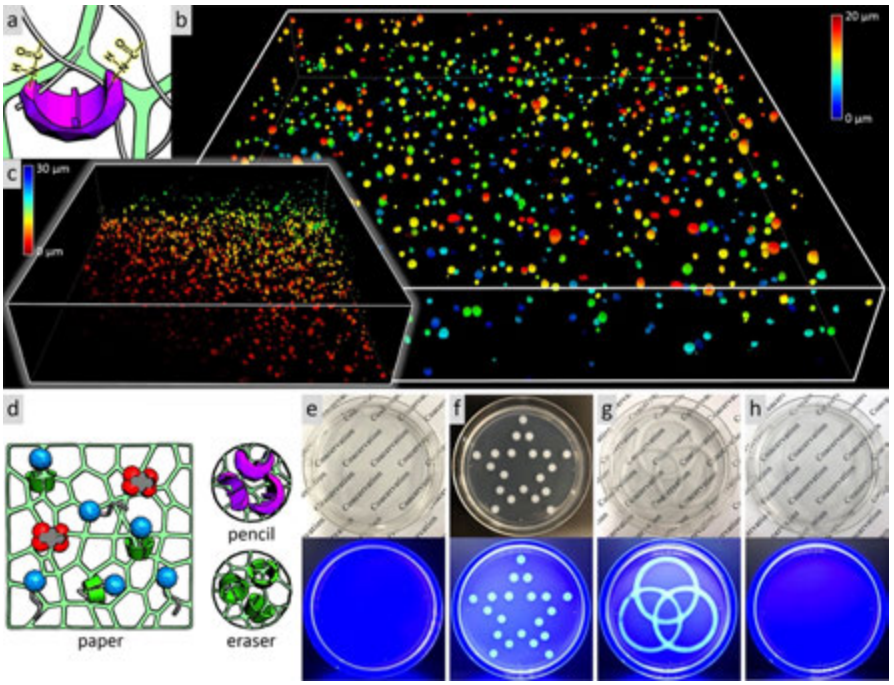

Figure 3. Spatially controlled coacervate formation in amylase-grafted hydrogels. (a) Amylase is grafted to a double-network hydrogel. (b) 3D confocal scan of the droplets formed in a DTAB/PTS/β-CD-loaded and amylase-grafted hydrogel. Scanning box = 150 × 150 × 20 μm. (c) Amylase grafting is localized to a 2 mm spherical region in a hydrogel such that droplet formation is also localized. Edge of the spherical region (120 × 120 × 30 μm) is scanned in 3D, where a clear transition from no droplet to abundant droplets can be observed. Color bars in (b,c) indicate height in z axis. (d) Schematic design for the paper-pencil-eraser system. (e–h) Pentagram (f) and three-circle (g) patterns are written on blank paper (e) and then erased (h). Top and bottom rows are pictures under white and UV light, respectively.

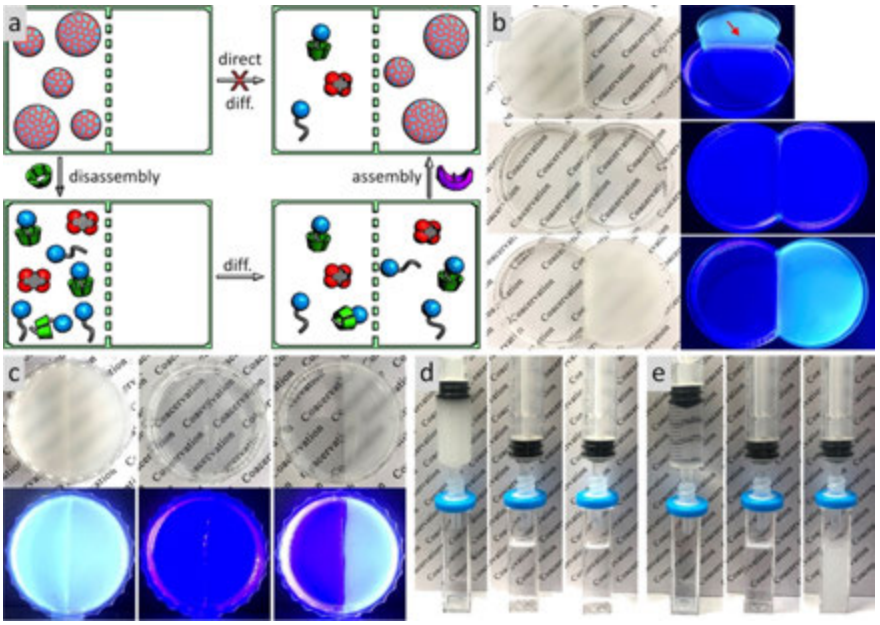

Figure 4. Disassemble-to-pass strategy. (a) Schematic illustration of the strategy, where large coacervate droplets have to be disassembled into monomers to pass through a semipermeable membrane and to be restored on the other side. (b) Experimental realization of the strategy. Top to bottom rows: DTAB/PTS droplets restrained to the left chamber by the membrane (denoted by the red arrow); droplets dissolved; droplets condensed in the right chamber. (c) Right half of the hydrogel is grafted with amylase. Initially uniformly distributed droplets are dissolved and then restored on the right half. (d) DTAB/PTS coacervate cannot pass through a 100 nm filter. (e) DTAB/PTS/β-CD monomers can pass through a filter and can then be turned into a coacervate suspension upon amylase treatment.

other half uncoated. Incubation of DTAB/PTS/β-CD solution in this chamber produced coacervate droplets that were spread at both halves rather than localized to the coated half. We reason that the monomers, regulators, and coacervate droplets would do unbounded Brownian motion in a free solution, disfavoring a specific spatial distribution. Noticing the crowded cellular environment full of filaments and membranes to localize regulatory proteins,[1] we seek an ideal hydrogel framework that

DOI: 10.1021/acsnano.8b09332
ACS Nano XXXX, XXX, XXX–XXX

fulfills the following criteria: does not impede coacervate formation, traps coacervate droplets in position once they grow into certain sizes, limits monomer diffusion, and provides a backbone to covalently graft amylase.

To this end, we synthesize acrylamide-modified amylase (Figures 3a and S5), copolymerize it with acrylamide and cross-linkers to produce a polyacrylamide-amylase network, and impose a second network of agarose to render the final hydrogel mechanically stable and water-nonswellable. The amylase-grafted hydrogel is further loaded with DTAB/PTS/β-CD, followed by incubation at 55 °C for enzymatic decomposition of β-CD. The incubation turns the hydrogel from transparent and fluorescently blue to turbid and fluorescently cyan, indicative of coacervation. Massive, stationary coacervate droplets (5−10 μm in diameter and roughly spherical in shape) are distributed evenly in the hydrogel (Figure 3b and Movie S3). The droplets remain stable against coalescence or sedimentation for weeks but do slowly age due to Ostwald ripening. Localization of amylase to a 2 mm spherical region of a hydrogel piece produces colocalized coacervate droplets (Figure 3c and Movie S4).

Then we design a paper-pencil-eraser system where a sheet of DTAB/PTS/β-CD-loaded, amylase-free hydrogel is a blank paper, a piece of amylase-grafted hydrogel is a pencil, and a piece of β-CD-loaded hydrogel is an eraser (Figure 3d). Applying the pencil to the paper allows β-CD in the paper to continually diffuse into the pencil to be decomposed by amylase. Such decomposition generates localized coacervate droplets that produce turbid and fluorescently cyan trajectories. Applying the eraser to the trajectories releases β-CD locally to dissolve the coacervates, restoring the hydrogel transparency. This paper-pencil-eraser system would, in principle, enable us to create arbitrary shapes and patterns. For example, on blank paper (Figure 3e) is written a pentagram (Figure 3f) or a three-circle pattern (Figure 3g), and the patterns are then fully removed by the eraser (Figure 3h).

Disassemble To Pass Through. When we have to relocate bulky furniture to a new house, one way is to move it in one piece by powerful machines at a high cost, but a more convenient way would be to dismantle it into small pieces for transportation and to reassemble it at the destination. In the microscopic world, cells can afford the costly way of active transportation of large cargos by ATP-powered motor proteins in a crowded environment.[1] We demonstrate here a disassemble-to-pass strategy as schematically illustrated in Figure 4a, where coacervate droplets are too large to pass a membrane by direct diffusion, but a disassembly−reassembly detour would allow the cross-membrane transportation. In one experimental setup, DTAB/PTS coacervate droplets in the left chamber are restrained from the right by a semipermeable membrane in the middle (Figure 4b). Addition of β-CD to the left disassembles the droplets into monomers that can easily diffuse through the membrane to reach an equilibrium on both sides. Addition of amylase to the right cleaves β-CD molecules and produces droplets on the right. The transportation efficiency is dictated by monomer diffusion, where one disassembly/assembly cycle usually moves roughly 50% droplets to the other side and more cycles move more percentages. In another setup, the strategy is employed to transport the droplets across a hydrogel that would otherwise fix them in position (Figure 4c). A circular piece of hydrogel is grafted with amylase on the right half and is loaded with DTAB/PTS droplets uniformly. Infiltration of β-CD to both sides dissolves the droplets evenly as amylase is inactive at room temperature. Incubation of the hydrogel at 55 °C activates amylase that produces coacervate droplets on the right half.

Complementary to this strategy, one can further impose an external field (*e.g.*, electric, magnetic, or flow) on the monomers to migrate them along the gradient swiftly and efficiently. For example, a forced flow carries the DTAB/β-CD and PTS monomers across a filter completely in 1 min, and droplets are restored at the receiver by amylase. Specifically, pushing a DTAB/PTS coacervate suspension through a 100 nm filter traps all the coacervates in the filter and gives a clear solution (Figure 4d). Pushing a DTAB/PTS/β-CD solution through a filter traps nothing in the filter and gives a solution that can be turned into a coacervate suspension by amylase treatment (Figure 4e).

CONCLUSION

We demonstrated versatility of a regulator-based strategy in a synthetic model coacervation system: Spatially distributed formation of droplets was achieved in amylase-grafted hydrogels, and transportation across membranes and hydrogel networks were realized by a disassemble-to-pass strategy. Looking forward, we argue generality of the current strategy for synthetic self-assembly systems. First, CDs can interact with various hydrophobic moieties, and amylase serves specifically and efficiently to counteract CDs' effects. They are thus envisioned to be broad-spectrum regulators for a wide range of molecular assemblies, such as surface monolayers, micelles, vesicles, and fibers,[30,33] and nanoparticle−molecule hybrid structures.[34,35] Second, the patterning scheme here goes beyond the coacervate droplets to distribute assemblies like micelles and vesicles in space at will because the introduced hydrogel frameworks can fix the assemblies in position and limit monomer diffusion. It may even empower us to create a combination of spatially separated colonies of different assemblies, where intercolony communications can then be studied. Finally, the transportation scheme here is anticipated to be valid to a vast variety of smart systems responsive to different cues such as light, temperature, and pH.

EXPERIMENTAL SECTION

Materials. All chemicals purchased were of the highest available purity and were used as received. 1,3,6,8-Pyrenetetrasulfonic acid tetrasodium salt hydrate (PTS, ≥98%), α-amylase (~30 U/mg, from *Aspergillus oryzae*), and agarose (for molecular biology) were purchased from Sigma, USA. Dodecyltrimethylammonium bromide (DTAB, >98.0%) was purchased from TCI, Japan. Cyclodextrins (CDs, >98%), *N*-(3-(dimethylamino)propyl)-*N*′-ethylcarbodiimide hydrochloride (EDC, 98.0%), *N*-hydroxysuccinimide (NHS, 98.0%), acrylic acid (AAc, >99.7%), and acrylamide (AAm, >99.8%) were purchased from Aladdin, China. All aqueous solutions were prepared with 18.2 MΩ·cm deionized water produced by a Milli-Q System (Millipore, USA). Coacervate samples were prepared by weighing desired amount of powders into a buffer solution (20 mM sodium phosphate, 6.7 mM sodium chloride, pH 6.9 for amylase activity). The temperature was held at 55 °C for amylase to decompose CD and at 25 °C otherwise.

General Methods. Fluorescence spectra were acquired by a Hitachi F-4500 fluorescence spectrometer with excitation at 350 nm. Scattering light intensity and ζ-potential were measured by a Zetasizer NanoZS (Malvern, UK). Absorbance was acquired by an Agilent 8453 diode array UV−vis spectrophotometer. 2D slices or 3D *z*-stacks of the coacervate droplets were captured with a Leica TCS SP8 confocal microscope (60× oil objective, 1.4 NA). A 405 nm laser was used to excite DTAB/PTS coacervates.

Cryogenic Transmission Electronic Microscope. A few microliters of samples was mounted onto a lacey carbon copper film TEM grid, and the excess solution was removed with filter paper. The specimen was immersed into liquid ethane with the help of a cryo-box

DOI: 10.1021/acsnano.8b09332
ACS Nano XXXX, XXX, XXX−XXX

(Carl Zeiss Microscopy GmbH, Jena, Germany), to be rapidly cryofixed between −170 and −180 °C. The specimen was then transferred to a Zeiss/LEO EM922 Omega EFTEM (Zeiss Microscopy GmbH) by an Oxford cryo-transfer holder (CT3500, Gatan, Munich, Germany). TEM observation was made around −180 °C with an acceleration voltage of 200 kV. Reduced electron doses (500−2000 e nm^{-2}) were used to obtain zero-loss filtered micrographs. A bottom-mounted CCD camera system (UltraScan 1000, Gatan) was employed to record all images, which were then processed by GMS 1.9 (Gatan).

Epifluorescence Microscopy and Droplet Contour Tracking. We visualized the dissolution and condensation of coacervate droplets on glass surfaces using a Zeiss inverted epifluorescence microscope (Andor EMCCD camera) with a 100× oil objective. The field of view was 82 × 82 μm, and depth of focus was 1.5 μm. Videos were collected typically at 20 fps for 2000−3000 frames, which were then analyzed by IDL codes written in-house (Figure S6).

Synthesis of Amylase-Grafted Hydrogel. Amylase was first modified with acrylic acid. Typically, a mixture of amylase (25 mg), AAc (100 μL), and EDC (532 mg) in 5 mL of MES buffer (pH adjusted to 6.5 ± 0.2 with NaOH) was incubated ∼2 h for the reaction to finish. Unreacted AAc was washed off by dialysis (membrane cutoff MW 2000). The solution was freeze-dried and stored at 4 °C before use. The product was confirmed by FTIR and NMR. Second, the modified amylase was grafted to a double-network hydrogel. Typically, 5 mL of pregel aqueous solution that contained 0.75 wt % agarose, 5 wt % AAm, 0.019 wt % MBAA, and 0.2 wt % I2959 was heated at 90 °C until the agarose powder was dissolved. The pregel solution was cooled to 55 °C in a water bath, and 17 mg of AAc-modified amylase (30 U/mg) was added and mixed evenly. Then the resulting solution was injected into a mold to cool at room temperature so the agarose forms fibers that gel the sample. Finally, the sample was irradiated under UV light (365 nm, 100 W) for 10 min such that AAm, modified amylase, and MBAA were polymerized to form another network.

ASSOCIATED CONTENT

Supporting Information

The Supporting Information is available free of charge on the ACS Publications website at DOI: 10.1021/acsnano.8b09332.

Molecular structures (Figure S1), macroscopic pictures of coacervate samples (Figure S2), fluorescence spectra of PTS (Figure S3), enzymatic efficiency (Figure S4), synthesis of amylase-grafted gels (Figure S5), and droplet tracking protocol (Figure S6) (PDF)

Movie S1: Droplet dissolution from −6 to 4 s (AVI)

Movie S2: Droplet condensation from 0 to 150 s (AVI)

Movie S3: Uniformly distributed coacervate droplets in a hydrogel (AVI)

Movie S4: Locally distributed coacervate droplets in a hydrogel (AVI)

AUTHOR INFORMATION

Corresponding Authors

*E-mail: tumei@jnu.edu.cn.

*E-mail: jianglx@jnu.edu.cn.

ORCID

Yun Yan: 0000-0001-8759-3918

Steve Granick: 0000-0003-4775-2202

Lingxiang Jiang: 0000-0001-5848-3904

Author Contributions

S.Y. and L.J. conceived the experiment and wrote the manuscript. S.Y., B.L., and L.J. performed the experiments and analyzed the data. M.D. conducted cryo-TEM observations. All the authors contributed to discussing the results and writing the paper.

Notes

The authors declare no competing financial interest.

ACKNOWLEDGMENTS

L.J. acknowledges support by National Natural Science Foundation of China (No. 21773092), Guangdong Natural Science Funds for Distinguished Young Scholar (No. 2018B030306011), and the Fundamental Research Funds for the Central Universities (No. 21617320). S.G. acknowledges support by the Institute for Basic Science, Project Code IBS-R020-D1. M.D. is supported by the collaborative research center SFB840 of the German Science Foundation DFG.

REFERENCES

(1) Pollard, T. D.; Earnshaw, W. C.; Lippincott-Schwartz, J.; Johnson, G. *Cell Biology*; Elsevier Health Sciences, 2016.

(2) Brangwynne, C. P.; Eckmann, C. R.; Courson, D. S.; Rybarska, A.; Hoege, C.; Gharakhani, J.; Jülicher, F.; Hyman, A. A. Germline P Granules Are Liquid Droplets That Localize by Controlled Dissolution/Condensation. *Science* **2009**, *324*, 1729−1732.

(3) Philipp, B.; Dautzenberg, H.; Linow, K.-J.; Kötz, J.; Dawydoff, W. Polyelectrolyte Complexes—Recent Developments and Open Problems. *Prog. Polym. Sci.* **1989**, *14*, 91−172.

(4) Spruijt, E.; Cohen Stuart, M. A.; van der Gucht, J. Linear Viscoelasticity of Polyelectrolyte Complex Coacervates. *Macromolecules* **2013**, *46*, 1633−1641.

(5) Kim, S.; Huang, J.; Lee, Y.; Dutta, S.; Yoo, H. Y.; Jung, Y. M.; Jho, Y.; Zeng, H.; Hwang, D. S. Complexation and Coacervation of Like-Charged Polyelectrolytes Inspired by Mussels. *Proc. Natl. Acad. Sci. U. S. A.* **2016**, *113*, E847−E853.

(6) Priftis, D.; Xia, X.; Margossian, K. O.; Perry, S. L.; Leon, L.; Qin, J.; de Pablo, J. J.; Tirrell, M. Ternary, Tunable Polyelectrolyte Complex Fluids Driven by Complex Coacervation. *Macromolecules* **2014**, *47*, 3076−3085.

(7) Douliez, J. P.; Martin, N.; Gaillard, C.; Beneyton, T.; Baret, J. C.; Mann, S.; Beven, L. Catanionic Coacervate Droplets as a Surfactant-Based Membrane-Free Protocell Model. *Angew. Chem., Int. Ed.* **2017**, *56*, 13689−13693.

(8) Wang, M.; Wang, Y. Development of Surfactant Coacervation in Aqueous Solution. *Soft Matter* **2014**, *10*, 7909−7919.

(9) Keating, C. D. Aqueous Phase Separation as a Possible Route to Compartmentalization of Biological Molecules. *Acc. Chem. Res.* **2012**, *45*, 2114−2124.

(10) Strulson, C. A.; Molden, R. C.; Keating, C. D.; Bevilacqua, P. C. RNA Catalysis through Compartmentalization. *Nat. Chem.* **2012**, *4*, 941−946.

(11) Priftis, D.; Leon, L.; Song, Z.; Perry, S. L.; Margossian, K. O.; Tropnikova, A.; Cheng, J.; Tirrell, M. Self-Assembly of α-Helical Polypeptides Driven by Complex Coacervation. *Angew. Chem.* **2015**, *127*, 11280−11284.

(12) Song, Y.; Shimanovich, U.; Michaels, T.; Ma, Q.; Li, J.; Knowles, T. P. J.; Shum, H. C. Fabrication of Fibrillosomes from Droplets Stabilized by Protein Nanofibrils at All-Aqueous Interfaces. *Nat. Commun.* **2016**, *7*, 12934.

(13) Song, Y.; Michaels, T. C. T.; Ma, Q.; Liu, Z.; Yuan, H.; Takayama, S.; Knowles, T. P. J.; Shum, H. C. Budding-Like Division of All-Aqueous Emulsion Droplets Modulated by Networks of Protein Nanofibrils. *Nat. Commun.* **2018**, *9*, 2110.

(14) Levin, A.; Michaels, T. C. T.; Adler-Abramovich, L.; Mason, T. O.; Müller, T.; Zhang, B.; Mahadevan, L.; Gazit, E.; Knowles, T. P. T. Elastic Instability-Mediated Actuation by a Supra-Molecular Polymer. *Nat. Phys.* **2016**, *12*, 926−930.

(15) Koga, S.; Williams, D. S.; Perriman, A. W.; Mann, S. Peptide−Nucleotide Microdroplets as a Step towards a Membrane-Free Protocell Model. *Nat. Chem.* **2011**, *3*, 720−724.

(16) Bhatia, S. R.; Khattak, S. F.; Roberts, S. C. Polyelectrolytes for Cell Encapsulation. *Curr. Opin. Colloid Interface Sci.* **2005**, *10*, 45−51.

DOI: 10.1021/acsnano.8b09332
ACS Nano XXXX, XXX, XXX−XXX

(17) Mann, S. Systems of Creation: the Emergence of Life from Nonliving Matter. *Acc. Chem. Res.* **2012**, *45*, 2131−2141.
(18) Shin, Y.; Brangwynne, C. P. Liquid Phase Condensation in Cell Physiology and Disease. *Science* **2017**, *357*, No. eaaf4382.
(19) Wei, M.-T.; Elbaum-Garfinkle, S.; Holehouse, A. S.; Chen, C. C.-H.; Feric, M.; Arnold, C. B.; Priestley, R. D.; Pappu, R. V.; Brangwynne, C. P. Phase Behaviour of Disordered Proteins Underlying Low Density and High Permeability of Liquid Organelles. *Nat. Chem.* **2017**, *9*, 1118−1125.
(20) Saha, S.; Weber, C. A.; Nousch, M.; Adame-Arana, O.; Hoege, C.; Hein, M. Y.; Osborne-Nishimura, E.; Mahamid, J.; Jahnel, M.; Jawerth, L.; et al. Polar Positioning of Phase-Separated Liquid Compartments in Cells Regulated by an mRNA Competition Mechanism. *Cell* **2016**, *166*, 1572−1584.
(21) Griffin, E. E.; Odde, D. J.; Seydoux, G. Regulation of the MEX-5 Gradient by a Spatially Segregated Kinase/Phosphatase Cycle. *Cell* **2011**, *146*, 955−968.
(22) Lee, C. F.; Brangwynne, C. P.; Gharakhani, J.; Hyman, A. A.; Jülicher, F. Spatial Organization of the Cell Cytoplasm by Position-Dependent Phase Separation. *Phys. Rev. Lett.* **2013**, *111*, 088101.
(23) Aumiller, W. M., Jr; Keating, C. D. Phosphorylation-Mediated RNA/Peptide Complex Coacervation as a Model for Intracellular Liquid Lrganelles. *Nat. Chem.* **2016**, *8*, 129−137.
(24) Aumiller, W. M., Jr; Pir Cakmak, F.; Davis, B. W.; Keating, C. D. RNA-Based Coacervates as a Model for Membraneless Organelles: Formation, Properties, and Interfacial Liposome Assembly. *Langmuir* **2016**, *32*, 10042−10053.
(25) Jiang, L. X.; Huang, J. B.; Bahramian, A.; Li, P. X.; Thomas, R. K.; Penfold, J. Surface Behavior, Aggregation and Phase Separation of Aqueous Mixtures of Dodecyl Trimethylammonium Bromide and Sodium Oligoarene Sulfonates: the Transition to Polyelectrolyte/Surfactant Behavior. *Langmuir* **2012**, *28*, 327−338.
(26) Ball, R. C.; Essery, R. L. H. Spinodal Decomposition and Pattern Formation Near Surfaces. *J. Phys.: Condens. Matter* **1990**, *2*, 10303−10320.
(27) Jiang, L.; Yan, Y.; Huang, J. Versatility of Cyclodextrins in Self-Assembly Systems of Amphiphiles. *Adv. Colloid Interface Sci.* **2011**, *169*, 13−25.
(28) Yang, S.; Yan, Y.; Huang, J.; Petukhov, A. V.; Kroon-Batenburg, L. M. J.; Drechsler, M.; Zhou, C.; Tu, M.; Granick, S.; Jiang, L. Giant Capsids from Lattice Self-Assembly of Cyclodextrin Complexes. *Nat. Commun.* **2017**, *8*, 15856.
(29) Jiang, L.; Yan, Y.; Huang, J.; Yu, C.; Jin, C.; Deng, M.; Wang, Y. Selectivity and Stoichiometry Boosting of β-Cyclodextrin in Cationic/Anionic Surfactant Systems: When Host− Guest Equilibrium Meets Biased Aggregation Equilibrium. *J. Phys. Chem. B* **2010**, *114*, 2165−2174.
(30) Jiang, L.; Yan, Y.; Drechsler, M.; Huang, J. Enzyme-Triggered Model Self-Assembly in Surfactant−Cyclodextrin Systems. *Chem. Commun.* **2012**, *48*, 7347−7349.
(31) Park, C.; Kim, H.; Kim, S.; Kim, C. Enzyme Responsive Nanocontainers with Cyclodextrin Gatekeepers and Synergistic Effects in Release of Guests. *J. Am. Chem. Soc.* **2009**, *131*, 16614−16615.
(32) Mahammad, S.; Abdala, A.; Roberts, G. W.; Khan, S. A. Manipulation of Hydrophobic Interactions in Associative Polymers Using Cyclodextrin and Enzyme. *Soft Matter* **2010**, *6*, 4237−4245.
(33) Lombardo, D.; Kiselev, M. A.; Magazù, S.; Calandra, P. Amphiphiles Self-assembly: Basic Concepts and Future Perspectives of Supramolecular Approaches. *Adv. Condens. Matter Phys.* **2015**, *2015*, 1−22.
(34) Kalsin, A. M.; Fialkowski, M.; Paszewski, M.; Smoukov, S. K.; Bishop, K. J. M.; Grzybowski, B. A. Electrostatic Self-Assembly of Binary Nanoparticle Crystals with a Diamond-Like Lattice. *Science* **2006**, *312*, 420−424.
(35) Nagarajan, R. *Self -Assembly: From Surfactants to Nanoparticles*; Wiley-Blackwell, 2018.

DOI: 10.1021/acsnano.8b09332
ACS Nano XXXX, XXX, XXX−XXX